Role of tensor interaction as salvation of cluster structure in ^{44}Ti

Chikako Ishizuka
Laboratory for Zero-Carbon Energy, Institute of Innovative Research, Tokyo Institute of Technology, 2-12-1-N1-9, Ookayama, Meguro-ku, Tokyo 152-8550, Japan

Hiroki Takemoto
Faculty of Pharmacy, Osaka Medical and Pharmaceutical University, 4-20-1, Nasahara, Takatsuki, Osaka 569-1094, Japan

Yohei Chiba
Department of Physics, Osaka City University, Osaka 558-8585, Japan; Nambu Yoichiro Institute of Theoretical and Experimental Physics (NITEP), Osaka City University, Osaka 558-8585, Japan; and Research Center for Nuclear Physics (RCNP), Osaka University, Ibaraki 567-0047, Japan

Akira Ono
Department of Physics, Graduate School of Science, Tohoku University, 6-3, Aramaki Aza-Aoba, Aoba-ku, Sendai 980-8578, Japan

Naoyuki Itagaki
Yukawa Institute for Theoretical Physics, Kyoto University, Kitashirakawa Oiwake-Cho, Kyoto 606-8502, Japan

(Received 22 February 2022; revised 24 May 2022; accepted 14 June 2022; published 24 June 2022)

The ^{44}Ti nucleus is believed to have a ^{40}Ca $+\alpha$ cluster structure; however, α (^{4}He) cluster structure tends to be washed out when we allow its breaking due to the spin-orbit interaction. Nevertheless, α clustering in medium-heavy nuclei is a popular subject recently. The tensor interaction plays an essential role in the strong binding of the ^{4}He, which induces the two-particle–two-hole (2p2h) excitation. Since this tensor effect is blocked when another nucleus approaches, it becomes the salvation of the ^{40}Ca $+\alpha$ clustering in ^{44}Ti. The competition of spin-orbit and tensor effects is investigated in the medium-heavy region for the first time.

DOI: 10.1103/PhysRevC.105.064314

I. INTRODUCTION

Owing to its distinctly large binding energy, ^{4}He becomes a good subsystem called an α cluster in the nuclear systems. Not only in the light-mass region, but also in the medium-heavy region, the α cluster structure has been investigated. From the theoretical side, the ^{44}Ti nucleus has been predicted to have a ^{40}Ca $+\alpha$ cluster structure [1], and experimentally, the inversion doublet structure has been observed [2,3], which supports the existence of cluster structure. The cluster structure of ^{44}Ti is also important in nuclear astrophysics; ^{44}Ti is one of the key elements for explosive nucleosynthesis in core-collapse supernovae and the ^{40}Ca$(\alpha,\gamma)^{44}$Ti reaction has been considered to be the main source for the production [4].

Until now, various theoretical models have been developed for the description of the cluster structures. For instance, resonating group method (RGM) has been applied to many two-body or three-body cluster systems [5]. To describe the nature of the second 0^+ state of ^{12}C, the so-called Hoyle state, Tohsaki-Horiuchi-Schuck-Röpke (THSR) wave function has been successfully applied [6]. Cluster structure can be justified even without assuming the existence beforehand; antisymmetrized molecular dynamics (AMD) [7] and fermionic molecular dynamics (FMD) [8] are powerful methods to describe the cluster states using all the nucleons' degrees of freedom independently.

In a simple description with an α cluster wave function, the contribution of the noncentral interactions (spin-orbit and tensor interactions) vanishes owing to the spin and isospin saturation. It is, however, widely known that one of the noncentral interactions, the spin-orbit interaction, is important in explaining the magic numbers of 28, 50, and 126 of the jj-coupling shell model [9]. If we allow the breaking of the α cluster(s), the cluster and shell structures compete with each other due to the spin-orbit interaction [10]. For instance, in ^{44}Ti, when we activate the degrees of freedom of four nucleons outside the ^{40}Ca core based on AMD, the α cluster structure is washed out due to the strong spin-orbit interaction, and they perform independent particle motions [11,12]. A similar discussion was made also for ^{48}Ti, showing that the calculated reduced width amplitude of α cluster structure is the order of magnitude smaller than the one expected from the experiment [13]. Therefore, how the α cluster structure survives in the medium-heavy region is quite an important subject, and many efforts have been devoted both from the theoretical and experimental sides [14,15].

To quantitatively discuss the cluster–shell competition transparently, we have developed antisymmetrized quasicluster model (AQCM) [16–29], which enables us to smoothly transform α-cluster model wave functions to jj-coupling shell model ones even within a single Slater determinant. The spin-orbit effect is included by breaking α clusters with a control parameter Λ in this model, and such clusters that feel spin-orbit interaction are called quasiclusters. The cluster-shell competition can be described with the parameter Λ and the distance(s) between clusters.

The first-order effect of another noncentral interaction, the tensor interaction, can be estimated by AQCM. However, more important tensor contribution comes from the inclusion of high-momentum components of the 2p2h states, which is included by using a different model, *i*SMT, also developed by us [30]. By applying *i*SMT to the four-α cluster structure of ^{16}O, the tensor interaction has been shown to increase the distances among α clusters. This is because the 2p2h excitation of α cluster(s) is blocked when other α clusters approach, and the attractive tensor contribution is suppressed. As a result, the tensor interaction works to keep the relative distances between clusters. This *i*SMT was reformulated as high-momentum antisymmetrized molecular dynamics [31], AQCM-T [32,33], and it has been possible to explain the mechanism of the α-α clustering in ^{8}Be starting with a realistic nucleon-nucleon interaction. An essential role is played by the tensor suppression effect at short relative distances.

In this study, we discuss the competition of the spin-orbit and tensor contributions in ^{44}Ti. The spin-orbit contribution is included by AQCM, which works to wash out the cluster structure. The tensor contribution is included by *i*SMT, which enhances the relative distance between clusters. The tensor interaction is found to be the salvation of the cluster structure.

II. MODEL

Both in AQCM and *i*SMT, the single-particle wave function has a Gaussian shape [34];

$$\phi_i = \left(\frac{2\nu}{\pi}\right)^{\frac{3}{4}} \exp[-\nu(\boldsymbol{r}_i - \boldsymbol{\zeta}_i)^2]\eta_i, \tag{1}$$

where η_i represents the spin-isospin part of the wave function and $\boldsymbol{\zeta}_i$ is a parameter representing the center of a Gaussian wave function for the ith particle. In the traditional cluster model (Brink model), the values $\boldsymbol{\zeta}_i = \boldsymbol{R}$ are common for four nucleons with different spin and isospin, which is the definition of the α cluster. We give different $\boldsymbol{R}$ values for other clusters if they exist, and the ^{40}Ca core is constructed with ten α clusters with small (0.2 fm) relative distances. After the antisymmetrization, it becomes identical to the closed-shell configuration of the shell model.

For the inclusion of the spin-orbit effect, we adopt AQCM. The four nucleons in the α cluster outside of the ^{40}Ca core is transformed into jj-coupling shell model based on the AQCM, by which the contribution of the spin-orbit interaction due to the breaking of α clusters is included. Here the $\boldsymbol{\zeta}_i$ values are changed to complex numbers. When the original value of the Gaussian center parameter $\boldsymbol{\zeta}_i$ is $\boldsymbol{R}$, which is real and related to the spatial position of this nucleon, it is transformed by adding the imaginary part as

$$\boldsymbol{\zeta}_i = \boldsymbol{R} + i\Lambda \boldsymbol{e}_i^{\text{spin}} \times \boldsymbol{R}, \tag{2}$$

where $\boldsymbol{e}_i^{\text{spin}}$ is a unit vector for the intrinsic-spin orientation of this nucleon. The control parameter Λ is associated with the breaking of the cluster, and two nucleons with opposite spin orientation have $\boldsymbol{\zeta}_i$ values that are complex conjugate to each other. This situation corresponds to the time-reversal motion of two nucleons. After this transformation, the α cluster is called a quasicluster. The four nucleons are transformed to the $(f_{7/2})^4$ configuration of the jj-coupling shell model at the limit of $|\boldsymbol{R}| \to 0$ and $\Lambda = 1$, when the ^{40}Ca core is located at the origin.

For the inclusion of the tensor contribution coming from the 2p2h excitation to the high-momentum states, we adopt *i*SMT [30]. The tensor interaction has a feature that the second-order effect is much stronger than the first-order one; therefore 2p2h configurations are important. To incorporate such configurations in *i*SMT, the Gaussian center parameters for the four nucleons in ^{4}He (in the example that ^{4}He is located at $\boldsymbol{R}$) are shifted by adding the imaginary parts in the following way;

$$\begin{aligned}
\boldsymbol{\zeta}_{p\uparrow} &= \boldsymbol{R} + id\boldsymbol{e}_z, \\
\boldsymbol{\zeta}_{n\uparrow} &= \boldsymbol{R}, \\
\boldsymbol{\zeta}_{p\downarrow} &= \boldsymbol{R}, \\
\boldsymbol{\zeta}_{n\downarrow} &= \boldsymbol{R} - id\boldsymbol{e}_z.
\end{aligned} \tag{3}$$

Here, the Gaussian center parameters of proton spin-up ($\boldsymbol{\zeta}_{p\uparrow}$) and neutron spin-down ($\boldsymbol{\zeta}_{n\downarrow}$) are shifted, with the parameter d taken to be 1.5, 3.0, ..., 15.0 fm (10 Slater determinants in addition to $d = 0$ fm). The spin orientation is quantized along the z axis, and $\boldsymbol{e}_z$ is a unit vector for this axis. We also prepare the basis states, where neutron spin-up ($\boldsymbol{\zeta}_{n\uparrow}$) is shifted instead of neutron spin-down. Eventually, we superpose these 21 Slater determinants in total. Here, the value of d can be considered as generate coordinate, and we optimize the coefficients for the linear combination of the 21 Slater determinants with different d values based on the generator coordinate method (GCM); the coefficients for the linear combination are determined by diagonalizing norm and Hamiltonian matrices.

In the original version, SMT, the real part was shifted to describe them; however, the effect has been quite insufficient [35]. On the other hand, in the improved version of SMT (*i*SMT) explained above, the imaginary part of the Gaussian center parameters is shifted instead of the real part. This is much suited for describing the high-momentum components since the imaginary part of Gaussian center parameter directly corresponds to the nucleon momentum.

The Hamiltonian ($\hat{H}$) consists of kinetic energy ($\hat{T}$) and potential energy ($\hat{V}$) terms, and the center-of-mass kinetic energy, which is constant, is subtracted. The potential energy has central ($\hat{V}_{\text{central}}$), spin-orbit ($\hat{V}_{\text{spin-orbit}}$), tensor ($\hat{V}_{\text{tensor}}$), and the Coulomb parts.

For the central part of the nucleon-nucleon interaction ($\hat{V}_{\text{central}}$), in many conventional cluster studies, the Volkov interaction [36] has been often used as the effective

TABLE I. The parameter set for the central part of the nucleon-nucleon interaction ($\hat{V}_{\rm central}$) adopted in the calculation [Eq. (4)] developed by one of the authors (H.T.).

α	V_α (MeV)	μ_α (fm)	M_α
1	611.88	0.81	−0.06979
2	−287.21	1.62	0.55326
3	57.972	2.43	0.68020

nucleon-nucleon interaction. Although this interaction is capable of describing various properties of light nuclei, it consists of only two ranges and is not designed to well describe the medium-heavy region. In the present case, if we adjust the Majorana exchange parameter to reproduce the binding energy of ^{40}Ca, it gives a too deep binding between ^{4}He and ^{40}Ca with a very small distance between them, which is not consistent with a well-developed cluster structure, even before taking into account the breaking of the α cluster. On the other hand, if we change the Majorana parameter to adjust the binding energy of ^{44}Ti from the ^{40}Ca + ^{4}He threshold energy, the ^{40}Ca + ^{4}He cluster structure does appear (if we do not include the breaking of the α cluster), but then the internal energy of ^{40}Ca becomes very underbinding. The internal binding energy of ^{40}Ca is indeed not explicitly needed in the actual calculation, but the obtained results are unreliable if this value is quite different from the experimental value. Therefore, we need to adopt an alternative nucleon-nucleon interaction suitable for describing the medium-heavy nuclei. Here we introduce the one developed by one of the authors (H.T.), which has three ranges:

$$\hat{V}_{\rm central} = \frac{1}{2}\sum_{i\neq j}\sum_{\alpha=1}^{3} V_\alpha \exp\left[-(\boldsymbol{r}_i-\boldsymbol{r}_j)^2/\mu_\alpha^2\right](W_\alpha + M_\alpha P^r)_{ij}. \tag{4}$$

Here, $P^r = -P^\sigma P^\tau$ represents the exchange of spatial part of the wave functions of interacting two nucleons, and $W_\alpha = 1 - M_\alpha$, where M_α is Majorana exchange parameter. The parameters are listed in Table I. This interaction is designed to reproduce the properties in a wide mass-number range. For instance, for the symmetric nuclear matter, the interaction gives the saturation point at the binding energy $E/A = -15.6$ MeV and the Fermi momentum $k_F = 1.29$ fm^{-1}. Also, it gives the incompressibility of $K = 239$ MeV.

For the spin-orbit part ($\hat{V}_{\rm spin\text{-}orbit}$), Gaussian three-range soft-core (G3RS) interaction [37], which is a realistic interaction originally determined to reproduce the nucleon-nucleon scattering phase shift, is adopted:

$$\hat{V}_{\rm spin\text{-}orbit} = \frac{1}{2}\sum_{i\neq j} V_{ij}^{ls}, \tag{5}$$

$$V_{ij}^{ls} = V_{ls}(e^{-d_1(\boldsymbol{r}_i-\boldsymbol{r}_j)^2} - e^{-d_2(\boldsymbol{r}_i-\boldsymbol{r}_j)^2})P(^3O)\boldsymbol{L}\cdot\boldsymbol{S}. \tag{6}$$

For the strength, $V_{ls} = 1600$–2000 MeV has been suggested to reproduce the scattering phase shift of ^{4}He and n [38]. We adopt $V_{ls} = 1800$ MeV, which reproduces various properties of ^{12}C [24,29]. This strength is suited for calculations without the tensor interaction. However, there has been discussion that the tensor interaction also contributes to the observed spin-orbit splitting of ^{4}He + n [39,40], and thus this strength $V_{ls} = 1800$ MeV can be considered as the maximum value (i.e., the genuine spin-orbit interaction must be weaker than this value).

For the tensor part ($V_{\rm tensor}$), we use Furutani interaction [41]. This interaction nicely reproduces the tail region of the one-pion-exchange potential.

The size parameter ν of the single-particle wave function is chosen to be 0.13 fm^{-2}, which gives the optimal energy (−339.51 MeV) and a reasonable radius [root mean square (rms) matter radius of 3.38 fm] for ^{40}Ca. We add one α cluster outside the ^{40}Ca core in ^{44}Ti.

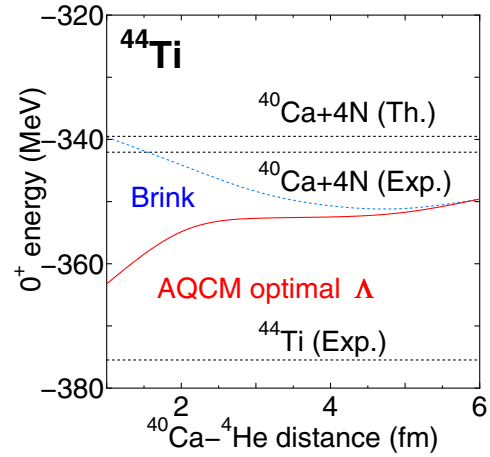

FIG. 1. Energy curves for the 0^+ state of ^{44}Ti as a function of the distance between ^{4}He and ^{40}Ca. The dotted curve is for the α + ^{40}Ca cluster model (Brink model) and the solid curve is the result of AQCM, where the optimal Λ value is adopted for each distance.

III. RESULTS

The energy curves for the 0^+ state of ^{44}Ti are shown in Fig. 1 as a function of the distance between quasicluster (^{4}He) and ^{40}Ca. The dotted curve is for the α + ^{40}Ca cluster model (Brink model, $\Lambda = 0$) and the solid curve is the result of AQCM, where the optimal Λ value is adopted for each distance. The horizontal dotted line at −339.51 MeV noted as ^{40}Ca + 4N (Th.) shows the theoretical ^{40}Ca + 4N threshold energy. Experimentally, the ^{40}Ca nucleus has the energy of −342.05 MeV noted as ^{40}Ca + 4N (Exp.) and ^{44}Ti is bound from this threshold by 33.42 MeV (the dotted line at −375.47 MeV shows the experimental ground-state energy of ^{44}Ti). There is no spin-orbit contribution for the dotted curve (Brink model), which has the energy minimum around the relative distance of ≈ 4 fm, and the binding energy there is much less than the experimental value (33.42 MeV below the threshold). On the other hand, in the solid curve, AQCM, the α cluster can be broken by introducing the Λ parameter, which is variationally determined, and the spin-orbit contribution is properly included. This effect is especially large at the short distances between ^{40}Ca and ^{4}He. The binding becomes deeper than the dotted curve (Brink model) with decreasing the relative distance, where the binding energy approaches the

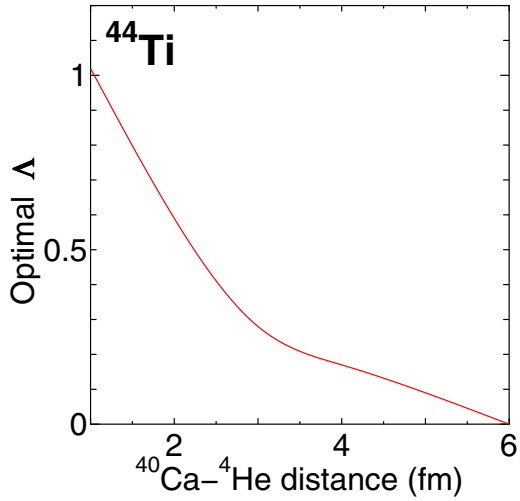

FIG. 2. Optimal Λ value of AQCM introduced to the ^{4}He cluster outside of the ^{40}Ca core for the 0^+ state of ^{44}Ti as a function of the distance between quasicluster (^{4}He) and ^{40}Ca.

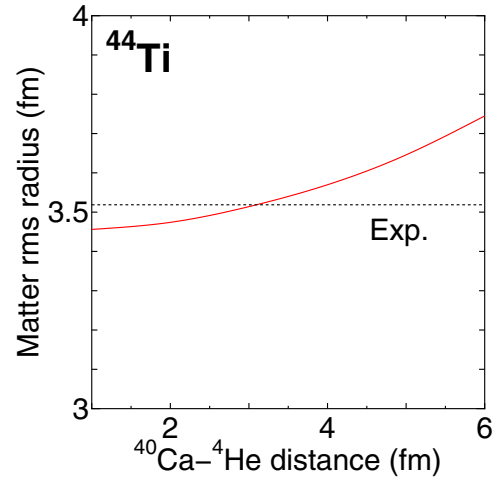

FIG. 3. Calculated rms matter radius for the 0^+ state of ^{44}Ti as a function of the distance between ^{4}He and ^{40}Ca. The optimal Λ value of AQCM is adopted for each distance.

experimental value. This means that the α cluster structure is significantly destroyed by the spin-orbit interaction when we allow the breaking of the α cluster, and thus the result indicates that the jj-coupling shell model state may be realized in the ground state of ^{44}Ti.

This possibility is confirmed by the optimal Λ value of AQCM, which is introduced for the ^{4}He cluster outside of the ^{40}Ca core. The adopted Λ value for the 0^+ state of ^{44}Ti is shown in Fig. 2 as a function of the distance between ^{4}He and ^{40}Ca. The value becomes almost unity at small relative distances, the α cluster structure is found to be completely washed out, and the four nucleons are changed into independent particles with the $(f_{7/2})^4$ configuration of the jj-coupling shell model. On the other hand, when the relative distance increases, the Λ value decreases and the difference between the α cluster model and AQCM becomes small.

The calculated rms matter radius for the 0^+ state of ^{44}Ti is shown in Fig. 3 as a function of the relative distance between ^{4}He and ^{40}Ca. The optimal Λ value of AQCM is adopted for each distance. Experimentally, the rms charge radii of ^{40}Ca and ^{44}Ti are 3.4776(19) and 3.6115(51) fm, respectively. The difference is 0.134 fm. In our model, the rms matter radius of ^{40}Ca is 3.38 fm, which is quite consistent with the experimental charge radius (the charge radius is deduced as 3.48 fm by using the proton radius of 0.81 fm). Here we face one problem; to explain this increase of the rms radius from ^{40}Ca to ^{44}Ti (experimentally 0.134 fm), the distance between ^{4}He and ^{40}Ca must have a certain value. According to AQCM, the lowest energy of ^{44}Ti is obtained at the relative distance of 1 fm and α cluster structure vanishes, but this relative distance of 1 fm gives a small rms radius. The figure tells us that we need ≈ 3 fm as the distance between the two clusters to explain the observed increase of the rms radius from ^{40}Ca to ^{44}Ti. This means that the cluster structure must survive to some extent in the ground state of ^{44}Ti. The experimental matter radius of ^{44}Ti can be deduced as 3.519 fm (dotted line) from the measured charge radius, and it crosses with the calculated result (solid line) around the intercluster distance of 3 fm.

Therefore, as the next step, we investigate the possibility of the tensor effect as the salvation of the cluster structure. We introduce *i*SMT and include the tensor effect. The energy of the 0^+ state of ^{44}Ti is shown in Fig. 4 as a function of the distance between ^{4}He and ^{40}Ca. Here again, the horizontal dotted lines noted as ^{40}Ca $+4N$ (Th.) and ^{40}Ca $+4N$ (Exp.) represent the theoretical and experimental ^{40}Ca $+4N$ threshold energies, respectively, and the one at -375.47 MeV shows the experimental ground-state energy of ^{44}Ti. The solid curve is the result of *i*SMT, and again, the dotted curve is for the $\alpha +$ ^{40}Ca cluster model (Brink model). The tensor effect becomes almost zero at the limit of a small distance between the two clusters (tensor suppression effect), but α cluster model and *i*SMT give quite different results at large relative distances.

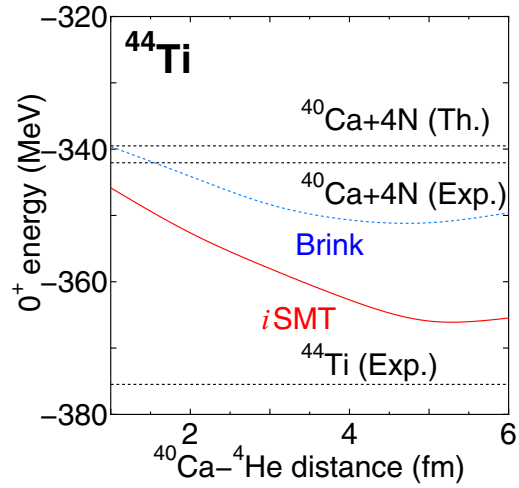

FIG. 4. Energy of the 0^+ state of ^{44}Ti as a function of the distance between ^{4}He and ^{40}Ca. The dotted curve is for the $\alpha +$ ^{40}Ca cluster model (Brink model) and the solid curve is the result of *i*SMT.

This means that the tensor suppression effect disappears at large relative distances. The minimum energy of *i*SMT is given around the relative distance of 5 fm. It can be confirmed that the tensor interaction induces the clustering of the system. Here, the minimum energy in *i*SMT (−365.92 MeV at the relative distance of 5 fm) is lower than that in AQCM (−363.22 MeV at 1 fm), which was discussed previously. Therefore, in the ground state of ^{44}Ti, it is considered that completely different structures of the jj-coupling shell model (AQCM) and ^{4}He + ^{40}Ca clustering (*i*SMT) contribute. If we mix two configurations with equal weight, the experimentally observed difference of radii between ^{40}Ca and ^{44}Ti could be reproduced.

As already explained, AQCM was introduced for the inclusion of the spin-orbit effect, whereas *i*SMT allows us to include the 2p2h excitation to high momentum states and resultant tensor effect. For an estimation of the coupling effect of these two, we solve the Hill-Wheeler equation; AQCM is represented by the basis state with the ^{40}Ca - ^{4}He distance of 1 fm with the optimal Λ (−363.22 MeV), while *i*SMT is by the distance of 5 fm (−365.92 MeV). They have the calculated rms matter radii are 3.46 and 3.63 fm. After coupling these states, two 0^+ states are obtained at −366.18 MeV and −362.92 MeV. The rms matter radius of the lowest state is 3.61 fm, and the increase from the ^{40}Ca one of 0.23 fm is overestimated compared to the experimental one (0.134 fm). Experimentally, the second 0^+ state is observed at E_x = 1.90 MeV. The present level spacing of 3.3 MeV for the two 0^+ states is larger than this value. These results would suggest that cluster configuration mixes slightly stronger than reality, and thus we have to perform more detailed investigations. For instance, the central interaction should be reconsidered after switching on the tensor interaction. In addition, the basis states of AQCM with the relative intercluster distance less than 1 fm should be included, and more states with different intercluster distances should be superposed. Also, the double projection has to be performed during the angular momentum projection process. These effects are expected to reproduce more precisely the ground-state energy compared to the experiment.

Finally, we consider the consistency between the central and tensor parts of the interaction. In the previous part, the tensor interaction was just added to the central interaction. However, the central interaction should be modified after introducing the tensor term by subtracting the doubly counted component; tensor interaction is renormalized in the triplet-even channel of the central part. In Refs. [32,33], we developed modified Volkov no. 2 interaction, where the triplet-even channel of the Volkov no. 2 interaction is reduced by 40% after inclusion of the tensor interaction, and the binding energy of ^{4}He is reproduced. In these studies, the spin-orbit interaction and tensor interaction were the original parameters of the G3RS interaction, which is a realistic interaction. Now we can apply this interaction set for the present analysis. The Volkov no. 2 interaction has one parameter, Majorana exchange parameter, and the binding energy of ^{4}He is insensitive to this value. Thus, we can tune this value to reproduce the binding energy of ^{44}Ti from the ^{40}Ca + ^{4}He threshold. The Majorana parameter of $M = 0.45$ is adopted, which gives good binding energy from the threshold, but the binding energy of ^{40}Ca is sacrificed (the binding is too weak). Therefore, here, only the binding of ^{44}Ti from the ^{40}Ca + ^{4}He threshold energy is discussed.

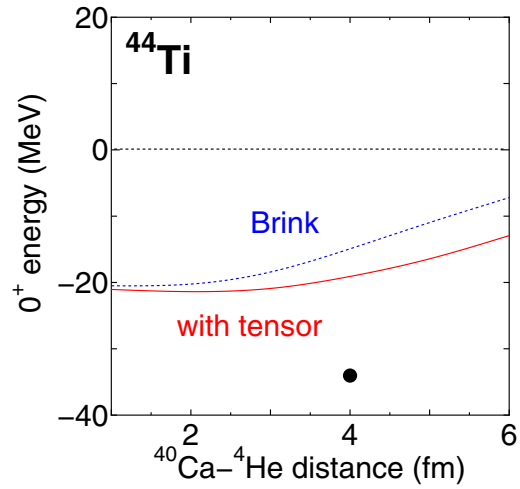

FIG. 5. 0^+ energy curves (dotted: Brink model, solid: *i*SMT) of ^{44}Ti measured from the ^{40}Ca + ^{4}He threshold as a function of the distance between ^{40}Ca and ^{4}He calculated with the modified Volkov no. 2 interaction for the central part and G3RS interaction for the spin-orbit and tensor terms. The solid circle shows the result of double angular-momentum projection at the relative distance of 4 fm.

Figure 5 shows the 0^+ energy curve of ^{44}Ti measured from the ^{40}Ca + ^{4}He threshold as a function of the distance between ^{40}Ca and ^{4}He calculated with the modified Volkov no. 2 interaction for the central part and G3RS interaction for the spin-orbit and tensor parts. The dotted line is for the Brink model, and the result shows that the energy minimum point appears at the zero distance limit between two clusters (shell-model limit). This is even before the inclusion of the breaking of the α cluster due to the spin-orbit interaction. On the other hand, the solid line is for the result of *i*SMT, where the tensor effect is included. The optimal distance between the two clusters is $\approx$ 3 fm. Thus, the tensor interaction indeed has the effect of enhancing the clustering.

One may think that if we include the α breaking effect due to the spin-orbit interaction using AQCM, the energy of the shell limit would become lower than the cluster state, and the cluster structure again disappears. While this may be true, the double projection effect contributes to the lowering of the cluster state with the tensor effect. Up to this point, we projected the angular momentum of only the total system; the ^{4}He nucleus was placed on the x axis, and the imaginary part of the Gaussian center parameters was given to the z components. In this case, the angular momentum of ^{4}He is not a good quantum number. If we mix the basis states, where the center of the ^{4}He is rotated on the xz plane, and perform the angular momentum projection of the total system, the angular momentum of the subsystem, ^{4}He, is restored in addition to the relative angular momentum between ^{40}Ca and ^{4}He. This procedure is called double projection. We generate the basis states, where the center of mass of ^{4}He is rotated around the y axis by 30° and 60°, and couple them with the original

basis states. When the ^{40}Ca - ^{4}He distance is 4 fm, this double projection effect lowers the energy by 15.1 MeV, which is shown as the solid circle in Fig. 5, and thus, the binding energy from the threshold energy (34.04 MeV) becomes reasonable compared with the experimental value (33.42 MeV). This effect disappears at short relative distances, and the double projection effect enhances the clustering. However, we need further investigations along this line.

IV. SUMMARY

In this article, the α cluster structure in the ^{44}Ti nucleus was investigated in the viewpoint of the cluster-shell competition. It is intriguing to point out that the tensor interaction works as the salvation of the cluster structure that could be otherwise destroyed by the spin-orbit interaction.

In the present study, at first, we just added the tensor interaction in the Hamiltonian. We also examined the case, where the central part is reduced after including the tensor term. The results are qualitatively unchanged, but the internal binding energy of ^{40}Ca is sacrificed in the latter case. Also, the double angular-momentum projection of subsystem (^{4}He) and total system is found to contribute to the lowering of the cluster states. These effects will be examined in more detail in the forthcoming work.

How to prove the existence of clustering is a big open question. In Japan, the experimental project to knockout α clusters from medium-heavy nuclei is ongoing. The observed cross sections can be directly related the theoretical spectroscopic factors. The study along this line is expected to be one on the major activities of the nuclear structure physics.

ACKNOWLEDGMENT

Numerical calculations have been performed at Yukawa Institute for Theoretical Physics, Kyoto University (Yukawa-21).

[1] F. Michel, G. Reidemeister, and S. Ohkubo, Phys. Rev. Lett. **57**, 1215 (1986).
[2] T. Yamaya, S. Oh-ami, M. Fujiwara, T. Itahashi, K. Katori, M. Tosaki, S. Kato, S. Hatori, and S. Ohkubo, Phys. Rev. C **42**, 1935 (1990).
[3] T. Yamaya, K. Katori, M. Fujiwara, S. Kato, and S. Ohkubo, Prog. Theor. Phys. Suppl. **132**, 73 (1998).
[4] H. Nassar, M. Paul, I. Ahmad, Y. Ben-Dov, J. Caggiano, S. Ghelberg, S. Goriely, J. P. Greene, M. Hass, A. Heger, A. Heinz, D. J. Henderson, R. V. F. Janssens, C. L. Jiang, Y. Kashiv, B. S. NaraSingh, A. Ofan, R. C. Pardo, T. Pennington, K. E. Rehm, G. Savard, R. Scott, and R. Vondrasek, Phys. Rev. Lett. **96**, 041102 (2006).
[5] Y. Fujiwara, H. Horiuchi, K. Ikeda, M. Kamimura, K. Katō, Y. Suzuki, and E. Uegaki, Prog. Theor. Phys. Suppl. **68**, 29 (1980).
[6] A. Tohsaki, H. Horiuchi, P. Schuck, and G. Röpke, Phys. Rev. Lett. **87**, 192501 (2001).
[7] A. Ono, H. Horiuchi, T. Maruyama, and A. Ohnishi, Phys. Rev. Lett. **68**, 2898 (1992).
[8] T. Neff and H. Feldmeier, Nucl. Phys. A **738**, 357 (2004).
[9] M. G. Mayer and H. G. Jensen, *Elementary Theory of Nuclear Shell Structure* (John Wiley and Sons, New York, 1955).
[10] N. Itagaki, S. Aoyama, S. Okabe, and K. Ikeda, Phys. Rev. C **70**, 054307 (2004).
[11] M. Kimura and H. Horiuchi, Nucl. Phys. A **767**, 58 (2006).
[12] Y. Chiba, M. Kimura, and Y. Taniguchi, Phys. Rev. C **93**, 034319 (2016).
[13] Y. Taniguchi, K. Yoshida, Y. Chiba, Y. Kanada-En'yo, M. Kimura, and K. Ogata, Phys. Rev. C **103**, L031305 (2021).
[14] S. Typel, G. Röpke, T. Klähn, D. Blaschke, and H. H. Wolter, Phys. Rev. C **81**, 015803 (2010).
[15] J. Tanaka, Z. Yang, S. Typel, S. Adachi, S. Bai, P. van Beek, D. Beaumel, Y. Fujikawa, J. Han, S. Heil *et al.*, Science **371**, 260 (2021).
[16] N. Itagaki, H. Masui, M. Ito, and S. Aoyama, Phys. Rev. C **71**, 064307 (2005).
[17] H. Masui and N. Itagaki, Phys. Rev. C **75**, 054309 (2007).
[18] T. Yoshida, N. Itagaki, and T. Otsuka, Phys. Rev. C **79**, 034308 (2009).
[19] N. Itagaki, J. Cseh, and M. Płoszajczak, Phys. Rev. C **83**, 014302 (2011).
[20] T. Suhara, N. Itagaki, J. Cseh, and M. Płoszajczak, Phys. Rev. C **87**, 054334 (2013).
[21] N. Itagaki, H. Matsuno, and T. Suhara, Prog. Theor. Exp. Phys. **2016**, 093D01 (2016).
[22] H. Matsuno, N. Itagaki, T. Ichikawa, Y. Yoshida, and Y. Kanada-En'yo, Prog. Theor. Exp. Phys. **2017**, 063D01 (2017).
[23] H. Matsuno and N. Itagaki, Prog. Theor. Exp. Phys. **2017**, 123D05 (2017).
[24] N. Itagaki, Phys. Rev. C **94**, 064324 (2016).
[25] N. Itagaki and A. Tohsaki, Phys. Rev. C **97**, 014307 (2018).
[26] N. Itagaki, H. Matsuno, and A. Tohsaki, Phys. Rev. C **98**, 044306 (2018).
[27] N. Itagaki, A. V. Afanasjev, and D. Ray, Phys. Rev. C **101**, 034304 (2020).
[28] N. Itagaki, T. Fukui, J. Tanaka, and Y. Kikuchi, Phys. Rev. C **102**, 024332 (2020).
[29] N. Itagaki and T. Naito, Phys. Rev. C **103**, 044303 (2021).
[30] N. Itagaki and A. Tohsaki, Phys. Rev. C **97**, 014304 (2018).
[31] T. Myo, H. Toki, K. Ikeda, H. Horiuchi, T. Suhara, M. Lyu, M. Isaka, and T. Yamada, Prog. Theor. Exp. Phys. **2017**, 111D01 (2017).
[32] H. Matsuno, Y. Kanada-En'yo, and N. Itagaki, Phys. Rev. C **98**, 054306 (2018).
[33] N. Itagaki, H. Matsuno, and Y. Kanada-En'yo, Prog. Theor. Exp. Phys. **2019** (2019) 063D02.
[34] D. M. Brink, Proc. Int. School Phys."Enrico Fermi" **XXXVI**, 247 (1966).
[35] N. Itagaki, H. Masui, M. Ito, S. Aoyama, and K. Ikeda, Phys. Rev. C **73**, 034310 (2006).
[36] A. Volkov, Nucl. Phys. **74**, 33 (1965).
[37] R. Tamagaki, Prog. Theor. Phys. **39**, 91 (1968).
[38] S. Okabe, Y. Abe, and H. Tanaka, Prog. Theor. Phys. **57**, 866 (1977).
[39] A. Arima and T. Terasawa, Prog. Theor. Phys. **23**, 115 (1960).
[40] T. Myo, K. Katō, and K. Ikeda, Prog. Theor. Phys. **113**, 763 (2005).
[41] H. Furutani, H. Horiuchi, and R. Tamagaki, Prog. Theor. Phys. **62**, 981 (1979).